Comparison of results of different methods for the analysis of flux creep behavior in a melt-textured $YBa_2Cu_3O_{7-x}$ sample showing a fishtail effect

M. Reissner and J. Lorenz

Institute of Applied and Technical Physics, Technical University of Vienna, A-1040 Vienna, Austria

(Received 30 December 1996)

Magnetic investigations of the flux creep behavior of a melt-textured $YBa_2Cu_3O_{7-x}$ sample with a pronounced fishtail effect are reported. To get information about the influence of oxygen on the pinning behavior, the sample was measured before and after a change in oxygen content by annealing. From the time dependence of the magnetic moment measured at fields of 1, 3, and 5 T and at temperatures between 4 and 72 K, the current density dependence of the effective activation energy was determined and interpreted in terms of collective pinning theory. The results are compared with those obtained from the simpler analysis within Anderson's flux creep theory, as well as with the results of an analysis in terms of activation energy distributions. Finally, measurements of the hysteresis loops recorded with different field sweep rates were analyzed using the ''generalized inversion scheme.'' The nature of the fishtail is discussed in comparison with existing models, which try to explain this effect. From all these analyses, a phase diagram for the pinning in the investigated sample is proposed, which is based on the assumption that two different types of pinning centers exist, which behave in different ways. Those that dominate in the field and temperature regime where no fishtail appears may be denoted as ''background'' pinning centers. They show a three-dimensional behavior with a change from small-flux-bundle pinning to large-flux-bundle pinning at higher temperatures. The pinning behavior in this field and temperature regime is not influenced by a change in the oxygen content. In contrast, the pinning centers that dominate in the field and temperature regime where the fishtail appears have higher activation energies and show a two-dimensional pinning behavior with a change from single vortex creep to collective vortex creep with increasing field and temperature. These pinning centers are strongly influenced by the oxygen content. [S0163-1829(97)09434-4]

I. INTRODUCTION

One phenomena in flux creep behavior of high-temperature superconductors (HTSC's) which still remains unclear is the appearance of a second peak—beside the central peak at $H=0$—in the field dependence of the critical current density J_c, which is called a ''fishtail'' and which is characterized by the fields H_{min}, where the critical current starts to rise, and H_{max}, where J_c reaches a maximum. This fishtail effect can be observed in nearly all kinds of HTSC's and has also been known to appear in low-temperature superconductors.[1] Its appearance seems to be not only independent of the type of superconductor, but also independent of the special type of sample, because it is found in single crystals, ceramics, films, grain-oriented, powdered, and melt-textured samples. It is also present in under- and overdoped as well as in irradiated samples with point or columnar defects. Corresponding to the numerous different samples with fishtails, there are numerous models which try to explain this effect. In the following some of these models, which are important for the discussion of our results, are briefly reviewed.

The first group of interpretations is based on the assumption that the fishtail is caused by inhomogeneities in the oxygen stoichiometry. In the granularity model[2] oxygen-deficient regions are assumed to become normal if the temperature is high enough. These normal regions increase in number and size with field and temperature. At H_{max}, these regions overlap, such that percolation sets in and leads

to granular behavior. In contrast, the Josephson-junction model[3,4] assumes, that currents between large regions of oxygen-poor material dominate at low fields. At H_{min} these regions start to decouple and above H_{max} they are all independent so that the magnetization is dominated by intra-regional currents. Another model assumes that the oxygen-deficient regions are microscopically small,[2,3,5,6] with a lower H_{c2} value than for the fully oxygenated matrix. At low fields the order parameter is only slightly suppressed leading to weak pinning centers, but with increasing field the order parameter of these regions is much more strongly suppressed than the order parameter of the matrix, thus making these pinning centers stronger with field. In many papers the influence of changing oxygen content on the fishtail behavior is discussed, but the role of oxygen is not quite clear. In many cases a correlation between fishtail and oxygen concentration is found. For example, in extremely pure (99.999%) $YBa_2Cu_3O_{7-x}$ (YBCO) single crystals it was shown that the fishtail can be reversibly suppressed by full oxygenation under high pressure.[7] There are also hints that not only the content but also the arrangement of the oxygen defects is important.[8,9] On the other hand, the second peak appears also in samples where oxygen defects play no role (e.g., $YBa_2Cu_4O_8$),[10,11] which leads to the assumption that other defects (e.g., impurities or structural defects like dislocations or stacking faults or strain fields around such defects) may be responsible for the fishtail.

In a quite different model, the fishtail is explained by a matching effect.[12] Here pinning is maximal due to a match-

ing of the vortex lattice with the impurity structure. At low fields the pinning centers are more dense than the vortices. The vortices can move relatively easily, because there are many energetically equivalent positions. At higher fields the vortex distance equals the mean defect spacing and the number of possible sites where the vortex can jump is reduced, which leads to enhanced pinning. Above H_{max} the current decreases because the order parameter is lowered near the irreversibility line.

A further model takes into account a possible softening of the tilt modulus of the flux-line lattice c_{44}. As Brandt[13,14] has pointed out, in real superconductors flux lines are usually pinned by more than one pinning center. In that case a soft flux-line lattice can be more strongly pinned than a rigid one. It was shown that phononlike fluctuations may play an important role by leading to a better adaption of the flux-line lattice to the defect structure.[15] In this interpretation the effect is expected to appear mainly near H_{c2}, because in that field range the order parameter decreases strongly with field.[1]

A growing number of authors favor a model where the increase of the critical current density with field is assumed not to be due to the appearance of field-induced pinning centers, but caused by some genuine changes in the flux-pinning properties.[10,16–20] The evidence for this hypothesis is in many cases a scaling of the bulk pinning force with temperature,[15,21] which points to the existence of only one single pinning mechanism. In the simple assumption of a static collective creep theory, an increase of the Larkin-Ovchinnikov correlation volume[22] with field could lead to fishtail behavior. In that case pinning would become stronger, because at higher fields the vortex distance is smaller leading to an increased vortex-vortex interaction and to long-range correlations. Also taking into consideration the strong time dependence of the magnetic moment, it was suggested[16,23] that the fishtail effect is connected to changes in the relaxation behavior at higher fields. Whereas the unrelaxed current density $J_c(t=0)$ decreases smoothly with increasing field, the anomalous increase of the relaxed current density $J_c(t)$ with field is caused by a lower relaxation rate at higher fields. In that case a minimum in the normalized creep rate S is expected where the maximum in $J_c(B)$ appears, because both would imply an increased pinning. Some authors have interpreted the fishtail effect by a dimensional crossover in the pinning behavior.[24–28] At low enough fields three-dimensional (3D) behavior is always expected, when the Josephson or magnetic coupling between the 2D vortices in different layers becomes stronger than the intraplane coupling, which fades out with increasing vortex distance. The 2D behavior in the fishtail regime can be concluded from the field dependence of the critical current density.

Finally, it was also mentioned that defects, like dislocations in the flux-line lattice itself, may cause the fishtail effect.[19] The elastic interaction between the flux-line lattice and the defect structure below the maximum in J_c may change into a plastic deformation of the flux-line lattice at higher fields, where consequently a saturation of the current density is observed.[29]

Depending on the type and quality of the sample there are quite different possible mechanisms which may produce fishtails in superconductors. If the sample's defect structure is more complex, more than one of these mechanisms may play a role in the formation of the fishtail. Especially complicated is the situation in melt-textured YBCO samples where a rich variety of defects are present. Melt-textured samples consist of a quasisingle crystalline $YBa_2Cu_3O_{7-x}$ (123) matrix with Y_2BaCuO_5 (211) inclusions. The good texture together with the presence of these 211 particles lead to current densities of more than 10^4 A/cm^2 at 77 K, which is much higher than in standard bulk material, and which makes these samples good candidates for a high current application of high-temperature superconductors.

In this paper we present magnetic flux creep measurements on such a melt-textured sample which shows the fishtail effect. Different methods of analysis are used to get information about the pinning behavior. It follows that the fishtail is related to the oxygen content in the sample, and that in terms of the collective pinning theory (CPT) the sample behaves in the field and temperature range where the fishtail appears in a two-dimensional way, whereas pinning is three dimensional at lower fields and temperatures.

The paper is organized as follows: in Sec. II experimental details concerning the preparation and microstructure of the sample and the magnetic measurements are given. In Sec. III the results of the magnetic measurements are presented. In Sec. IV the results of the static and in Sec. V of the dynamic relaxation measurements are analyzed. In Sec. VI the results are discussed and in Sec. VII conclusions are given.

II. EXPERIMENTAL

A. Sample preparation

A YBCO sample was prepared by the melt-texturing procedure.[30] YBCO powder from Rhône-Poulence was, after several heating steps in oxygen with intermediate grinding, pressed to a pellet by 250 MPa and sintered at 900 °C in oxygen. Next the sample was heated for five minutes to 1140 °C. During the following cooling (180 °C/h) to 1030 °C, the peritectic decomposition of 123 and 211 occured. Recrystallization of the 123 matrix happened during the following slow cooling (1 °C/h) down to 980 °C leading to well-textured grains of up to 130 mm^3. Afterwards the sample was cooled to 700 °C at 60 °C/h and finally furnace cooled to room temperature. The oxygenation of the sample took place at 450 and 400 °C, both for 45 h. The volume fraction of the 211 particles is 18%, and their mean diameter about 5 μm. They are homogeneously distributed in the 123 matrix, with density fluctuations, which have a periodicity of about 75 μm. Large stresses around the 211 particles could be identified. Planar defects with a mean spacing of 8 μm are found, which are parallel to the ab plane. There are also short randomly distributed microcracks around the inclusions. The density of the twins is highest near the 211 particles. The large grains consist of quadratic subgrains with very clean and crack-free boundaries. The tilting angle of the c axis of these subgrains against the mean c direction scatters around 6 degrees. Details of the microstructure of this sample were published by Diko, Pellerin, and Odier.[31] After carrying out the magnetic measurements, the oxygen content was increased by annealing the sample in flowing oxygen for 10 h at 550 °C, followed by 15 h at 500 °C, and finally 20 h at 450 °C. This procedure, called in the following ''reoxy-
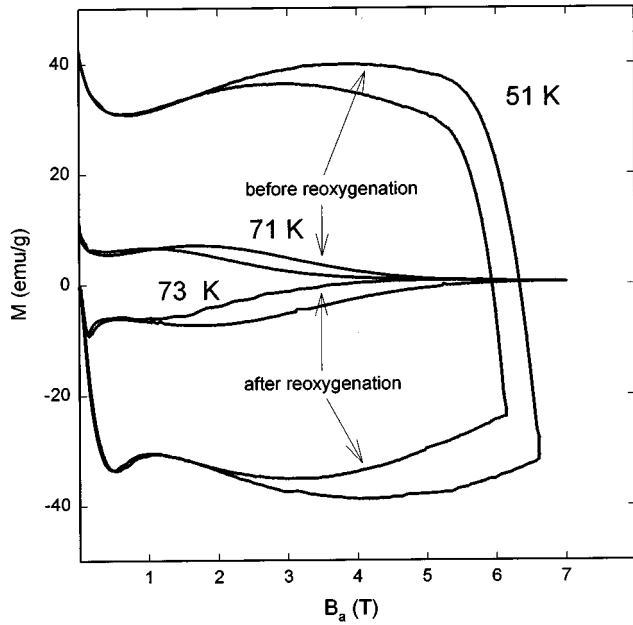
FIG. 1. Influence of a change in temperature and oxygen content on the shape of magnetic hysteresis loops.

genation,'' was performed to get information about the influence of the oxygen content on the pinning behavior.

B. Magnetic measurements

dc magnetic measurements were performed with a vibrating sample magnetometer (PAR 150A) in the temperature range 1.8–270 K in fields up to 7 T. For these measurements a rectangular sample with $a \times b \times c = 3.11 \times 1.16 \times 1.75$ mm^3 was prepared from a larger grain. The applied field B_a was always parallel to the mean c direction. The superconducting transition temperature T_c onset was found to increase from 88 to 89.6 K after the reoxygenation process. The transition width changed from 1.2 to 1.4 K. The higher T_c value indicates an increase in oxygen content after reoxygenation. The relatively low transition temperature before reoxygenation is due to the relatively short oxygenation process during sample preparation. Because of this low value a relatively large change in T_c and in the pinning behavior was achieved by the reoxygenation process. Due to the microcracks in the sample the distribution of the oxygen in the sample was on a large scale homogeneous, both before and after reoxygenation. This is indicated by the rather small transition width. After zero-field cooling to 4.2 K and heating the sample to the measuring temperature, hysteresis cycles with a field sweep rate of 3.9 mT/s were recorded. At 1, 3, and 5 T the field sweep was interrupted and the decay of magnetic moment with time was monitored for at least 30 min. During this relaxation the field was kept constant by switching the superconducting coil into persistent mode.

It has been shown[32–34] that the same information about the time dependence of the magnetic moment can also be obtained by a ''dynamic'' method, where hysteresis loops are recorded with different field sweep rates. This method has the advantage that (i) the field sweep does not have to be stopped for the relaxation measurements—such stopping might (especially at higher sweep rates) lead to a small over-
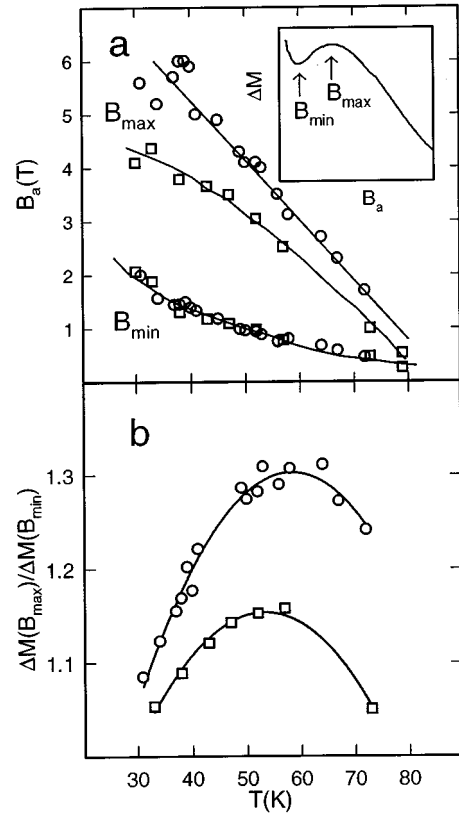

FIG. 2. Characterization of the fishtail by (a) the fields $B_{\min}$ and $B_{\max}$ and (b) by its relative strength $\Delta M(B_{\max})/\Delta M(B_{\min})$ measured before ($\bigcirc$) and after ($\square$) reoxygenation. Inset: Definition of the characteristic fields $B_{\min}$ and $B_{\max}$.

shoot of the field, which in turn leads to large changes in the relaxation behavior—and (ii) it is not necessary to hold both field and temperature constant for a long time as in the case of the relaxation experiments. For the analysis it is necessary to vary the sweep rate over a large range. However, because of the large inductance of the superconducting coil the sweep rate could only be varied in a limited interval. Nevertheless, such measurements were performed before reoxygenation of the sample. Hysteresis loops were recorded at different temperatures, where a few tenth of a Tesla in advance of 1, 3, and 5 T the sweep rate was reduced in two steps from 3.9 to 2.45 and 0.94 mT/s, and increased again shortly after passing these field values. This procedure made it possible to determine the change of the width of the hysteresis loops with decreasing sweep rate at 1, 3, and 5 T from one hysteresis loop. The waiting time after each step was long enough to ensure that the superconducting system could adjust to the new condition. This was checked at 4.2 K, where the thus obtained curves were compared with hysteresis loops, where the different sweep rates were hold constant during the whole cycle.

III. RESULTS

The hysteresis loops show a pronounced fishtail effect, which depends both on temperature and oxygen content. For example, in Fig. 1 hysteresis loops recorded at different temperatures before and after reoxygenation are shown. With
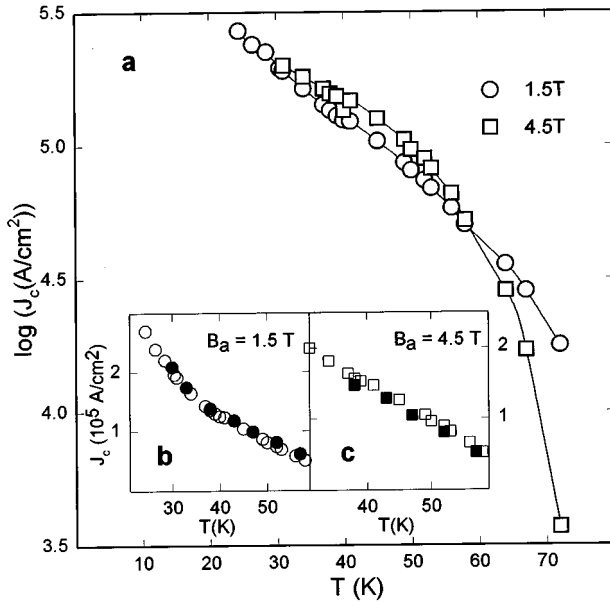
FIG. 3. Temperature dependence of the critical current density at different fields in logarithmic representation determined after Eq. (1) (a) and in linear representation at 1.5 T (b) and 4.5 T (c). Open symbols indicate measurements before and closed symbols indicate measurements after reoxygenation.

FIG. 4. Examples of the time dependence of the magnetization for the sample measured before reoxygenation at 5 T for selected temperatures.

increasing temperature the maximum width of the hysteresis shifts to lower fields. After reoxygenation the fishtail is less pronounced than before. The fishtail is characterized by two fields (inset, Fig. 2): B_{min} (denoting the field where the width of the hysteresis starts to increase) and B_{max} (where it has its maximum). Both the maximum field B_{max} [Fig. 2(a)], as well as the relative strength of the fishtail characterized by the relation $\Delta M(B_{max})/\Delta M(B_{min})$ [Fig. 2(b)], where ΔM is the width of the hysteresis at the respective field, are reduced after the reoxygenation, whereas the field B_{min} remains unchanged [Fig. 2(a)].

Magnetic measurements in low fields show full screening of the sample up to fields where, in untextured polycrystalline materials, the so-called weak-link hysteresis is usually found,[35,36] indicating that the sample behaves in a nongranular way. Therefore the critical current densities J_c could be determined by using the Bean formula for rectangular-shaped samples[37]

$$J_c(\text{A/cm}^2) = 40|M_{irr}|/[b(1-b/3a)], \quad (1)$$

where M_{irr} is the irreversible part of the magnetization, which is obtained from $M_{irr} = M - M_{rev}$ with $M_{rev} = (M\uparrow - M\downarrow)/2$, b the width and a the length of the sample. Because the main planar defects are oriented parallel to the ab plane, they do not disturb the current flow for measurements with applied fields parallel to the c direction. For example, values of 1.5×10^5 and 2.0×10^4 A/cm^2 were obtained for 35 and 70 K at 1 T before reoxygenation. In Fig. 3 the temperature dependence of the resulting critical current density is given. For $H=1.5$ T, an exponential decrease of J_c is obtained up to 70 K. Practically no influence of the reoxygenation process is found in this field regime [Fig. 3(b)]. At higher fields a hump in the temperature dependence
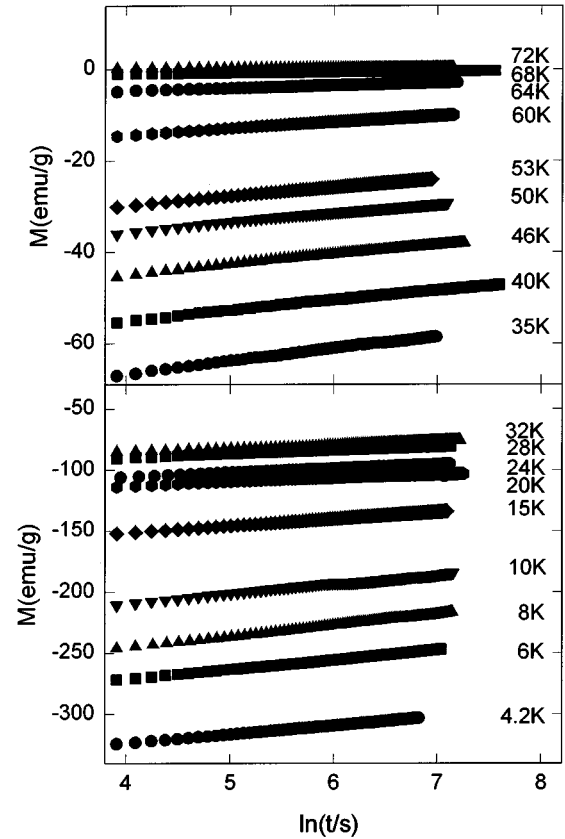
appears between ~30 and 55 K [Fig. 3(a)], indicating the fishtail regime. Due to the less pronounced fishtail, J_c is slightly reduced after reoxygenation at those high fields [Fig. 3(c)].

In Fig. 4 the time dependence of the magnetic moment measured at 5 T for several temperatures before reoxygenation is given. Within experimental accuracy, this time dependence is logarithmic in time in the investigated time window and allows the determination of a creep rate $dM/d\ln t$. From the vanishing of this creep rate the irreversibility temperature T_{irr} can be estimated. Before reoxygenation $T_{irr} = 84$, 79, and 76 K was found for $B_a = 1$, 3, and 5 T, respectively.

From the normalized creep rate $S = (dM/d\ln t)M_{irr}^{-1}$ a mean effective activation energy $\langle E \rangle$ can be determined using the flux creep theory of Anderson.[38,39] At low temperatures a small peak appears in the temperature dependence of S, which shifts to higher temperatures with decreasing field (left side of Fig. 5). After a flat dip S starts to strongly increase when approaching the irreversibility line. The start of the strong increase happens at temperatures, where the mean effective activation energy shows a maximum, which also shifts to higher temperatures for lower fields (right side of Fig. 5). The temperature dependence of the unnormalized creep rate shows a pronounced maximum at low temperatures (Fig. 6), which shifts to lower temperatures for higher fields. Because of the weaker temperature dependence of the critical current density in the melt-textured sample, this shift
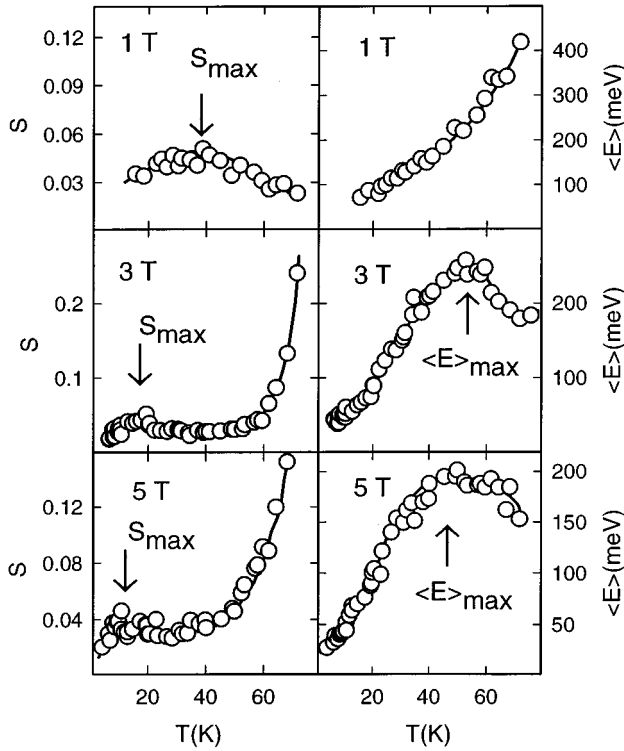
FIG. 5. Temperature dependence of the normalized creep rate S (left) and the mean effective activation energy $\langle E \rangle$ determined after Anderson (Refs. 38 and 39) (right) at 1, 3, and 5 T measured before reoxygenation.
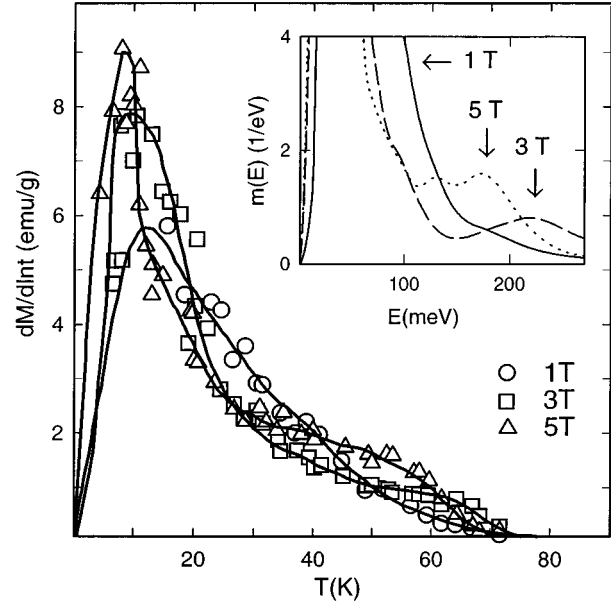

FIG. 6. Temperature dependence of the creep rate determined from measurements before reoxygenation at 1, 3, and 5 T. Inset: Activation energy distributions determined after Hagen, Griessen, and Salomons (Ref. 41) from the temperature dependence of the creep rate.

is smaller than usually found in untextured polycrystalline YBCO samples.[40] At higher temperatures a clear field dependent anomaly is visible, which can be related to the fishtail. Whereas for 1 T—a field below the onset of the fishtail—the creep rate is reduced smoothly with increasing temperature, a hump appears at higher fields, which is shifted to lower temperatures for increasing field (Fig. 6).

According to Hagen, Griessen, and Salomons[41] an activation energy distribution $m(E)$ can be determined from the temperature dependence of the unnormalized creep rate. Because this theory takes only thermal activation into account, the solid lines, which describe the temperature dependence of the unnormalized creep rate, are extrapolated to zero for $T = 0$. Within the investigated temperature interval no indication for an appearance of quantum creep is obtained. Due to the shoulder in the creep rate at higher temperatures, a broad peak appears in the distribution function at higher energies for 3 and 5 T, which is not visible at 1 T (inset, Fig. 6). The appearance of a second peak indicates that in the fishtail region, not an increased number, but a different type of pinning centers with higher activation energy dominates. Unlike the oversimplified model of Anderson, which takes into account only a single mean barrier height, the model of Hagen, Griessen, and Salomons[41] assumes a more realistic distribution of activation energies. However, this model also has major shortcomings, because it still uses the Anderson-Kim ansatz[38,39]

$$U = U_0 - |F|VX, \qquad (2)$$

where a linear relation between effective activation energy U and true pinning potential height U_0 is assumed to exist. V is the flux bundle volume and X is the hopping distance. The driving force $|F|$ is determined by the applied field and the field gradient in the sample and is proportional to the current density J. This linear $U(J)$ relation is very crude, because it implies a V-notch-like pinning potential.[42] For physically more realistic potential shapes, nonlinear $U(J)$ relations are the consequence. The Anderson-Kim relation is identical to the tangent on the real $U(J)$ curve at that current density, which corresponds to the momentary measuring conditions.[42] Therefore large differences may appear between the linearly extrapolated U_0 value and the real pinning potential barrier height.

As pointed out by Maley et al.[43] the true shape of the $U(J)$ relation can be determined by the relaxation data. Instead of introducing the linear ansatz Eq. (2) for the effective activation energy into the solution of the flux diffusion equation, which is for constant field and slab geometry given by

$$4\pi(dM/dt) = (2HX\nu_0/d)\exp(-U/kT), \qquad (3)$$

a rearrangement leads to

$$U = -kT(\ln|dM/dt| - C) \qquad (4)$$

with

$$C = \ln[HX\nu_0/(2\pi d)], \qquad (5)$$

where ν_0 is the attempt frequency for flux hopping and d the thickness of the slab. In plotting for different temperatures U/k versus M_{irr}, which is related to J via Eq. (1), the $U(J)$ relation can be determined for the different temperatures. The unknown parameter C, which is assumed to be temperature independent, is determined by the condition, that
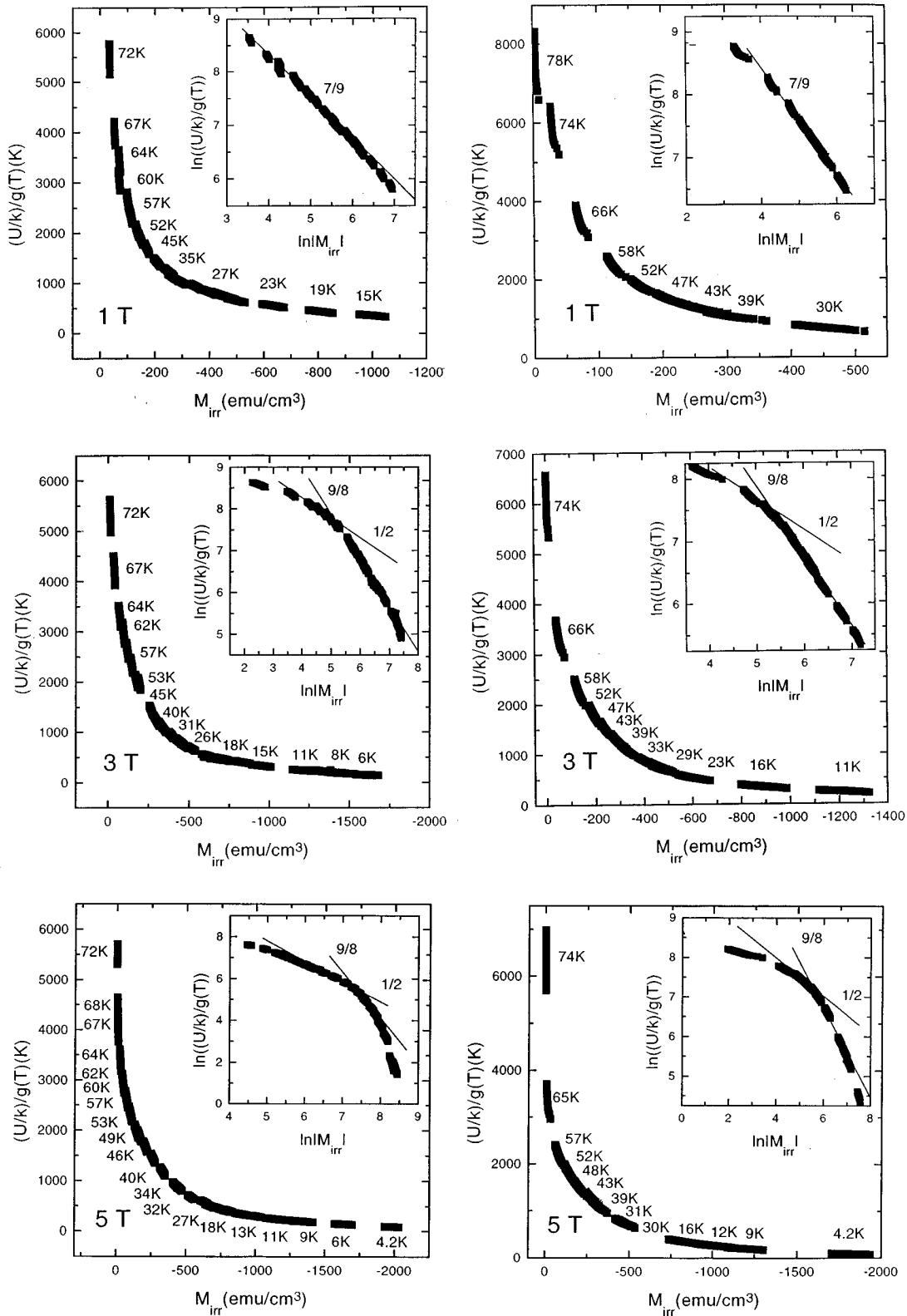
FIG. 7. Linear and double logarithmic (insets) representation of $(U/k)/g$ over irreversible magnetization, which is directly proportional to the current density, determined at 1, 3, and 5 T measured before (left) and after (right) reoxygenation.

all points for the different temperatures have to lie on one smooth curve. The smoothness can only be reached in the low-temperature region, because at higher temperatures a change in the pinning well height has to be taken into account. Following a suggestion by Tinkham[44] $g(T) \sim [1$

$-(T/T_K)^2]$ with $T_K = T_c$ was used. McHenry et al.[45] have obtained better results in using the irreversibility temperature T_{irr} instead of the transition temperature T_c, although no theoretical argument was given for this choice. In Fig. 7 the $U(J)$ relations for 1, 3, and 5 T are given, which were ob-
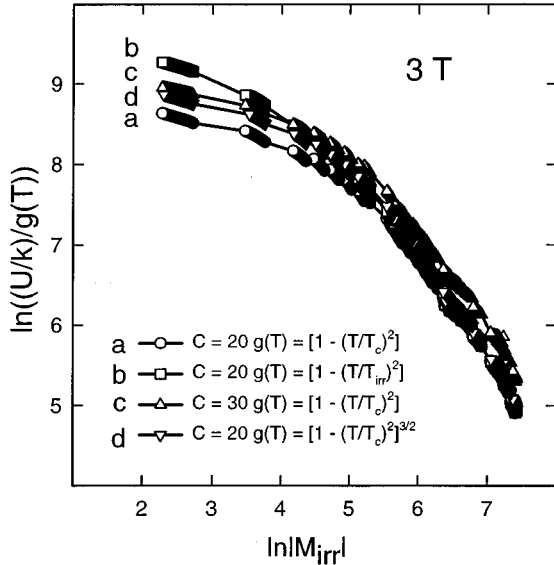
FIG. 8. $(U/k)/g$ determined at 3 T before reoxygenation analyzed by using different C and T_K values, as well as different functions for the temperature dependence $g(T)$ of the pinning potential.

tained before and after reoxygenation. All curves are calculated with $C=20$ and with $T_K=T_c$. Because it is only a logarithmic correction term, a variation of the C value changes the obtained $U(J)$ curves only slightly as shown in Fig. 8. Also the exchange of T_c by T_{irr} does not improve the result.

IV. ANALYSIS OF THE STATIC RELAXATION MEASUREMENTS

A logarithmic $U(J)$ dependence was proposed from the analysis of resistivity measurements for a variety of different superconductors by Zeldov et al.[46] A more general equation was suggested by Feigel'man et al.[47] working from the basis of the collective pinning theory, where the pinning of randomly distributed weak pinning centers is discussed by taking the elasticity of the flux-line lattice into account. This theory predicts for $J \ll J_c$ an inverse power law

$$U=U_c(J_c/J)^{\mu}, \qquad (6)$$

where U_c is the activation energy for $J=J_c$. The exponent μ depends upon the dimensionality and upon the particular flux creep regime. In the case of three-dimensional (3D) pinning $\mu=1/7$, 3/2, and 7/9 are proposed[47] for pinning of single vortices, of small flux bundles (sfb), and of large flux bundles (lfb), respectively. If ξ is smaller than the distance of the superconducting layers, flux decouples into pancakes, and two-dimensional (2D) pinning takes place. In that case $\mu=9/8$ and 1/2 are proposed[48,49] for single vortex (svc) and collective vortex creep (cvc), respectively. In a recent paper[50] it was shown that in the case of cvc a differentiation in small, medium, and large bundle pinning leads to $\mu=7/4$, 13/16, 1/2. An interpolation formula

$$U=U_c[(J_c/J)^{\mu}-1], \qquad (7)$$

which is valid for all J values, was given by Feigel'man, Geshkenbein, and Vinokur.[51] In the case of $\mu=-1$ the Anderson and of $\mu=0$ the Zeldov equation are obtained.

There are two ways of analyzing the experimentally determined $U(J)$ curves in terms of the collective pinning theory. One is to fit them by Eq. (7). In this case the full J region can be covered, but in the fit μ is constrained to be independent of the current density. If the system changes its pinning behavior with temperature, wrong μ values may be the result of such a fit. This can be checked by fitting the interpolation formula to different temperature intervals and by comparing the resulting μ values. The other possibility is to plot ln U over ln J. According to Eq. (6) μ appears as the slope in such a double logarithmic representation. A possible change of μ results in a deviation from linearity. However, this method has the disadvantage that it is only applicable for current densities which are much smaller than the critical current density, a condition which is normally fulfilled in most of the temperature range, because of the small field sweep rate used in the experiment, the true critical current density is never reached. The best proof is to fit just the low-temperature regime by the interpolation formula and to compare the resulting μ value with the slope at low temperatures, which appears in the double logarithmic plot.

In the insets of Fig. 7 the double logarithmic representation of the $U(J)$ relations is shown. For 1 T a line with slope 7/9 fits the data for nearly the whole temperature range. This corresponds to the pinning of large flux bundles in three dimensions. Only at low temperatures a line with steeper slope seems to fit the data better. The validity of this analysis was checked by fitting the interpolation formula to the curve [solid line in Fig. 9(a)]. Taking into account the whole temperature range, a value for the flux creep exponent μ of 0.71 is obtained, which confirms the result of the graphical analysis. In contrast to the results at 1 T, a strong bending of the $U(J)$ curves for 3 and 5 T is found in the double logarithmic representation (insets, Fig. 7). Now the data are represented much better by lines with slopes of 9/8 at low and 1/2 at high temperatures. This corresponds with the two-dimensional pinning behavior, where the system changes with the temperature from creep of single vortices (svc) to collective vortex creep (cvc). The change from svc to cvc appears at lower temperatures for 5 T than for 3 T. A fit of the $U(J)$ relations at 3 and 5 T after Eq. (7) fails. No single value for μ was found which could fit the whole temperature range satisfactorily. But if the $U(J)$ curves are divided into two temperature intervals, which are fitted separately, the same μ values are obtained as in the case of the graphical analysis [Fig. 9(b)].

A change from 3D behavior of pinning of large flux bundles at 1 T to single vortex pinning in two dimensions at 3 and 5 T is hard to understand. Therefore the data are checked in more detail in the following. In Fig. 10 the results of the graphical analysis of the $U(J)$ relations are given, which were performed both in such a way that it was assumed that the system behaves for all fields and temperatures in a three-dimensional or in a two-dimensional way. The area outside of the dotted lines indicates those temperatures and fields where no relaxation measurements were carried out. The horizontal bars indicate those temperature intervals, where linear dependences in the double logarithmic repre-
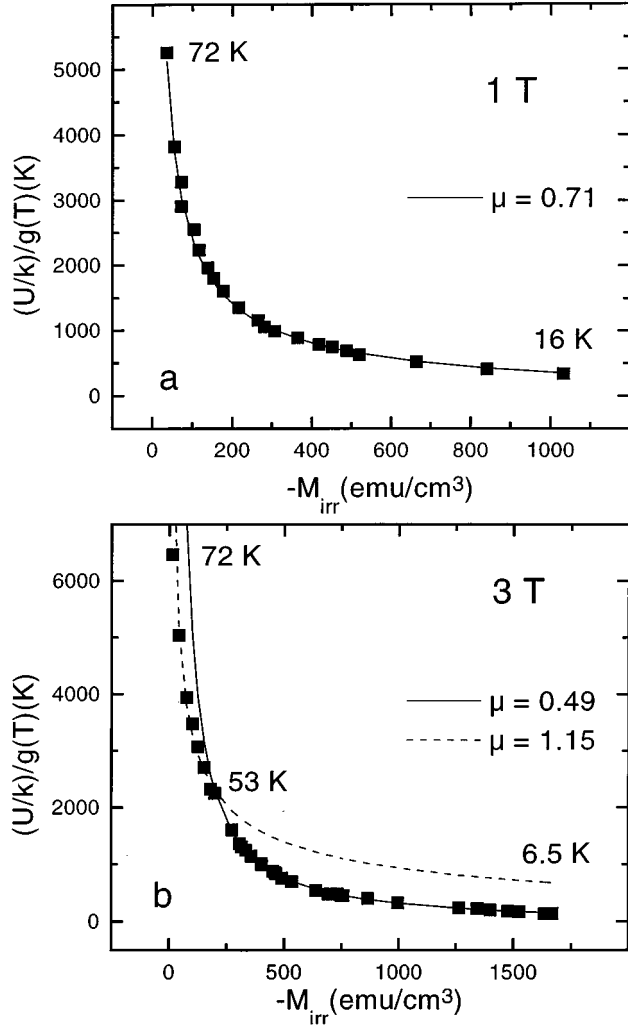
FIG. 9. Examples of fits of the $U(J)$ relations by the interpolation formula Eq. (7) performed at 1 T (a) and 3 T (b) before reoxygenation. In contrast to Fig. 7, for better visualization for each temperature only one data point, which was taken 100 s after starting the relaxation, is shown. At 1 T one unique μ value describes the full temperature range (16 to 72 K), whereas at 3 T no single fit was possible. The fit has therefore been performed in two different temperature intervals (above and below 53 K).

sentation are found, which correspond to distinct μ values. The results clearly indicate that the bars (and thus the corresponding temperature regimes) are longer in the 2D case for $B_a=3$ and 5 T, whereas for 1 T they are longer for the 3D case. Also the phase boundaries, which are found if a dimensional crossover is not accepted (dashed-dotted lines in Fig. 10) are contrary to the ones expected from theory,[52] where it is predicted that the system should change from single vortex creep to pinning of small flux bundles and further to pinning of large flux bundles both with increasing temperature and field. In view of this analysis one has to conclude that the system changes with increasing field from a 3D to a 2D behavior.

V. ANALYSIS OF THE DYNAMIC RELAXATION MEASUREMENTS

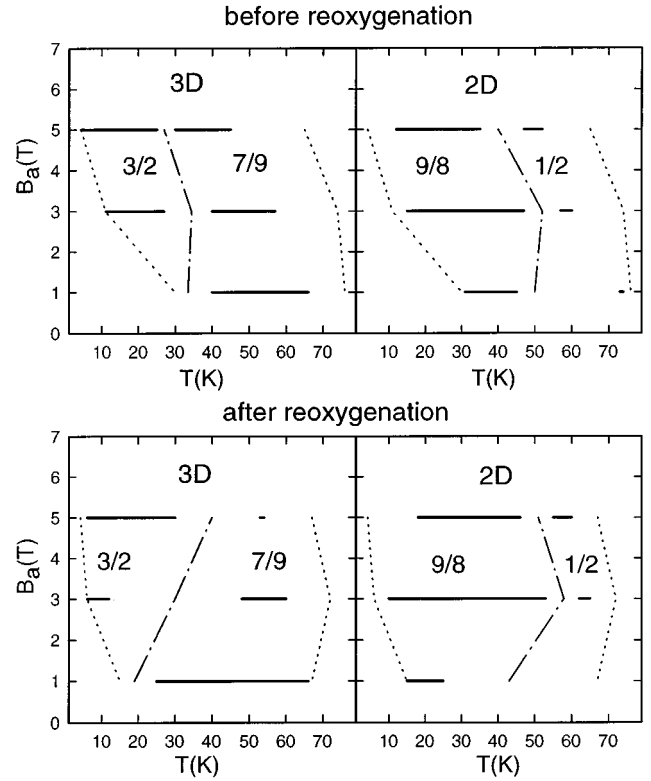Instead of the normalized creep rate S the dynamic relaxation rate[53]

FIG. 10. Analysis of the $U(J)$ curves of Fig. 7 in terms of the collective pinning theory (CPT) under the assumption that the pinning is in the full temperature and field range three-dimensional (left) or two-dimensional (right). The dotted lines indicate the range in which relaxation measurements were performed. The horizontal bars indicate those temperatures where a given μ value fits the $U(J)$ curves quite well. The dashed-dotted lines indicate the phase boundaries.

$$Q = d\ln J_c/d\ln(dB_a/dt) \qquad (8)$$

is determined from the sweep rate dependence of the width of the hysteresis loops. It can be shown that Q is closely related to S.[54] The change of the effective activation energy with current density can be written as

$$U(J) = C_g kT \qquad (9)$$

with $C_g \sim \ln[X\nu_0 B_a/d(dB_a/dt)]$, where d is the slab's thickness. C_g depends on field and sweep rate, as well as on sample geometry and is related to the constant C used in the analysis after Maley et al.[43] by

$$C_g \sim \ln|dM/dt| - C. \qquad (10)$$

Insertion of Eq. (7) into Eq. (9) and using Eq. (8) for Q leads, under the assumption that both U_c and μ are temperature independent, to

$$T/Q = U_c/k + \mu C_g T. \qquad (11)$$

In a T/Q vs T plot C_g can be determined as the slope in the low-temperature regime. U_c/k appears as the intersection at $T=0$. Schnack et al.[55] showed that C_g can also be determined without the assumption of a specific pinning model like the collective pinning theory Eq. (7), if it is assumed that

the current density and the explicit temperature dependence of the activation energy can be separated according to

$$U(J,T;B_a)=h(T;B_a)f(J/J_{ct}).\qquad(12)$$

J_{ct} is the true critical current density for which the activation energy vanishes and which is—like the apparent critical current density J_c, which is determined from experiment after Eq. (1)—also a function of both T and B_a. With this general ansatz it is possible to show,[55] that C_g appears as the slope at $T=0$ in a $-d\ln J_c/d\ln T$ vs Q/T plot. A further assumption in the model is that the temperature dependence of the characteristic pinning energy is related to the true critical current density by a power law

$$U_c\propto J_{ct}(T;B_a)^p,\qquad(13)$$

where the exponent p depends, like the flux creep exponent μ in Eqs. (6), (7), on both dimensionality and flux creep regime. A consideration[56] of the current dependence of the pinning potential leads to p values of 1 (1/2), $-1/2$ ($-3/2$), and $0(-1/2)$ for single vortex, small bundle, and large bundle pinning in 2D (3D), respectively.

In the ''generalized inversion scheme'' (GIS) the true critical current density J_{ct} can be determined from the temperature dependence of both the dynamic relaxation rate Q and the apparent critical current density J_c. With Eqs. (9) and (12) the temperature dependence of J_c is given by

$$J_{ct}(T)=J_c(0)\exp\int_0^T\frac{C_gQ(T')(1-d\ln G(T')/d\ln T')+d\ln J_c/d\ln T'}{1+pC_gQ(T')}\frac{dT'}{T'},\qquad(14)$$

where $G(T)=(1+t^2)^l(1-t^2)^m$ with $t=T/T_c$. l and m are determined by the temperature dependence of the prefactor in Eq. (13) which relates U_c to J_{ct}^p. Beside p, which fixes the parameters l and m, all quantities on the right-hand side of Eq. (14) are obtained from the experiment. The selection of the free parameter p for physically relevant results is discussed below.

Technically the integral in Eq. (14) is approximated by a summation allowing the calculation of the temperature dependence of J_{ct} by the recursion formula

$$J_{ct}(T_{i+1})=J_{ct}(T_i)\exp\frac{\ln[J_c(T_{i+1})/J_c(T_i)]+C_g/2\{\ln(T_{i+1}/T_i)-\ln[G(T_{i+1})/G(T_i)]\}[Q(T_{i+1})+Q(T_i)]}{1+0.5pC_g[Q(T_{i+1})+Q(T_i)]}\qquad(15)$$

for given p and C_g values.

One problem is that one has to find the value J_{ct} for the starting temperature T_0, which is usually the lowest temperature reached in the experiment. It can be determined by solving the integral Eq. (14) in the limits 0 to T_0. In order to do this it is necessary to find appropriate extrapolations for both $Q(T)$ and $J_c(T)$ for this low-temperature range. According to Eq. (11) $Q(T)$ can be approximated by a linear extrapolation of T/Q down to $T=0$. In contrast to this, the simple linear extrapolation of $\ln J_c$ to zero temperature is in contradiction to the collective pinning theory. Therefore a parabolic function obtained from integration of a linear extrapolation of $d\ln J_c/dT$ between $T=0$ and T_0 was used as proposed by Wen et al.[56] For $T=0$ one obtains $d\ln J_c/dT|_{T=0}=-kC_g/U_c$. Therefore with the knowledge of C_g and U_c the temperature dependence of J_c can be evaluated. Together with the extrapolated $Q(T)$ values Eq. (14) can be solved to get J_{ct} at T_0. With this value the temperature dependence of J_{ct} in the temperature range where experimental data for Q and J_c exist is calculated by using Eq. (15) for different p values. The curves obtained are then discussed in relation to their physical relevance in order to get the correct p value and the dominant pinning regime.

Because the field sweep rate could be varied only by a factor ~4 in the experiment, the precision of the obtained Q values was not high enough [Fig. 11(a)] to determine C_g with the necessary accuracy directly from the slope at low temperatures in the $d\ln J_c/dT$ vs Q plots, as proposed in the GIS. Therefore a different method of determining the correct p value and the dominant pinning regime was followed by starting the analysis with Eq. (11). In Fig. 11 (b), an example
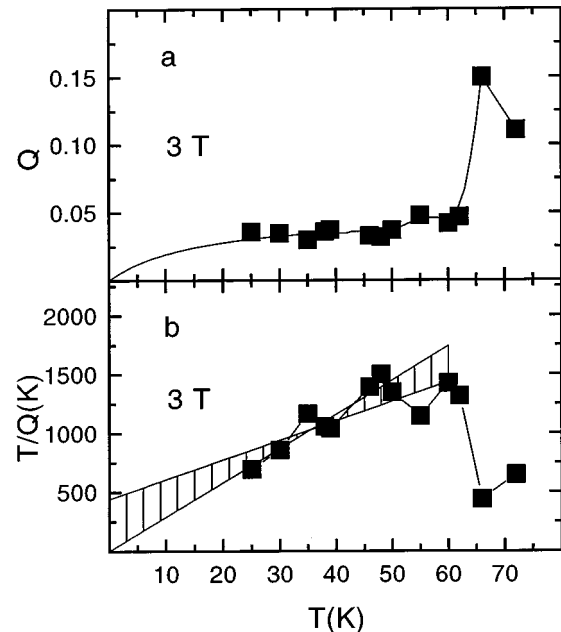
FIG. 11. (a) Temperature dependence of the dynamic creep rate for a field sweep rate of 3.9 mT/s measured at 3 T before reoxygenation. The low-temperature part of the line is calculated according to Eq. (11). (b) Temperature dependence of T/Q. According to Eq. (11) the slope on the low-temperature part of this curve gives μC_g. The shaded area indicates the range of lines, which are used as possible linear approximations of this low-temperature part of the curve.

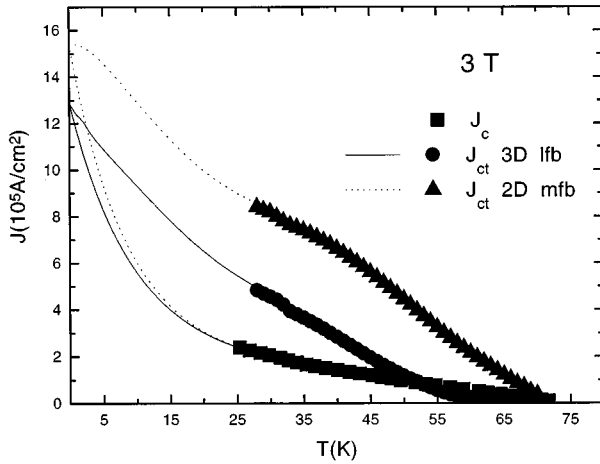FIG. 12. Temperature dependence of the true critical current density J_{ct} obtained by means of the generalized inversion scheme (GIS) for 3D creep of large flux bundles (*lfb*) and from 2D pinning of medium flux bundles (*mfb*) together with the measured induced current density J_c. The lines indicate the low-temperature extrapolations as described in the text.

of the temperature dependence of T/Q is given for 3 T. The shaded area indicates the range which can be used to approximate the low-temperature part within the experimental accuracy. The decrease of T/Q at high temperatures, which is due to thermal depinning, is ignored. The possible values for μC_g and U_c/k are restricted by the conditions $U_c > 0$ and $C_g > C$. For each of these pairs $J_{ct}(T)$ was determined according to the aforementioned inversion scheme for the different pinning regimes characterized both by specific μ and p values. $T_0 = 28$ K was chosen for the starting temperature. For a given μ value the constant C_g follows from the chosen value for μC_g. Together with the corresponding U_c value the temperature dependence of the apparent critical current density J_c below T_0 was determined. At zero temperature the true and the apparent critical current densities are equal. A further limitation for the value of C_g follows from the exclusion of unreasonable high J_{ct} values obtained from the extrapolation procedure. Within these restrictions $J_{ct}(T)$ was determined not only for the different p but also for different C_g values.

If the reasonable range is restricted for C_g to values between 20 and 30 and for $J_{ct}(0)$ to values below 1 $\times 10^7$ A/cm^2, the analysis shows that only two solutions can be found. These are 3D pinning of large flux bundles and 2D pinning of medium flux bundles (Fig. 12). In the first case J_{ct} becomes lower than J_c for $T > 52$ K, which is only possible in the flux-flow regime above T_{irr}. The second case is more reasonable, because J_{ct} becomes zero at about 73 K a temperature very close to T_{irr}. The curves in Fig. 12 are calculated with $C_g = 27$, which was finally assumed to be the most reasonable value. According to Eq. (9) C_g is given by $(U/k)T$, which can be extracted directly from the data in Fig. 7 before applying the correction function $g(T)$. Such an estimation gives $C_g \sim 27$ for 3 T. Similar results are obtained by analyzing the 1 T data. For 5 T the scatter in the $Q(T)$ data is too large to make such an analysis meaningful. Therefore no statement concerning field dependence can be given within this type of analysis.
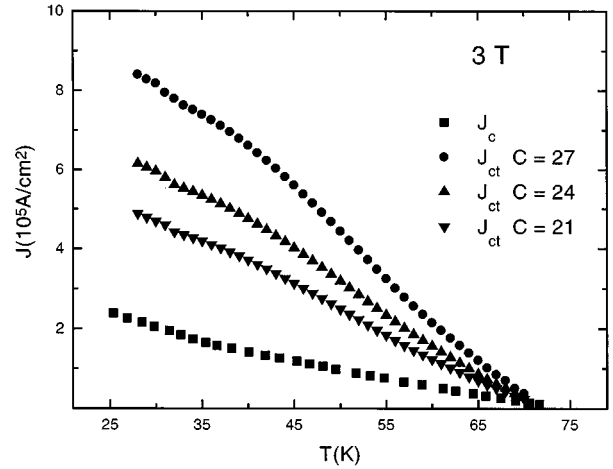

FIG. 13. Temperature dependence of the apparent critical current density J_c and of the true critical current density J_{ct} obtained by means of the generalized inversion scheme (GIS) for 2D creep of medium flux bundles calculated for different values of the parameter C_g. Whereas the value of $J_{ct}(T=0)$ is strongly changed by the different values of C_g, the shape and the temperature where J_{ct} becomes zero are relatively insensitive to this variation in C_g.

Nevertheless the analysis in terms of the GIS, like the analysis after Maley *et al.*,[43] points to 2D rather than to 3D pinning at high fields for the investigated sample. Whereas a variation in C_g leads to a relative large change in $J_{ct}(0)$, the shape of $J_{ct}(T)$ and the temperature where J_{ct} becomes zero are not strongly influenced as shown in Fig 13. Therefore a change in C_g will not alter the conclusions concerning the dimensionality of the pinning.

VI. DISCUSSION

The change from 3D to 2D behavior follows mainly from the analysis of the $U(J)$ curves by inspecting deviations from linearity in a double logarithmic representation. In many cases it was shown that such analysis gives physically reliable results. For example, in melt-textured YBCO samples which show 2D behavior because of strongly reduced oxygen content,[57] for $B_a \| c$ the 2D character is visible in the strong curvature of the $U(J)$ relation, whereas for $B_a \| ab$, where the vortices are parallel to the CuO$_2$ planes and therefore are not decoupled into pancakes, the $U(J)$ curves are straight lines with a slope of ~ 0.78 which corresponds to the expected 3D pinning of large flux bundles. The only problem in such an analysis is that the range $J \sim J_c$ is excluded. But usually for temperatures higher than 10 K such an analysis works well. This is comprehensible, because the true critical current density J_{ct} is about four times larger than the apparent critical current density J_c as shown in Fig. 12. Inclusion of the high-J regime is made possible by fitting the interpolation formula Eq. (7) to the $U(J)$ data. But in this case μ is kept constant in the temperature regime regarded in the analysis. A change in pinning behavior can therefore hardly be determined. In this case the obtained μ values are always only mean values, averaged over all pinning regimes present in the investigated temperature interval. The same problem arises in the analysis of the data within the generalized inversion scheme. Here the exponent which

is characteristic for a given flux creep regime is an input parameter for the analysis, which does not depend on temperature. Therefore the result can also only be regarded as a mean value over the investigated temperature range. Because in most of the investigated temperature intervals 2D behavior with a change from *svc* to *cvc* and only in the low-temperature regime 3D pinning is obtained, it is not unexpected that the only meaningful $J_{ct}(T)$ curve obtained from the analysis within the GIS gives 2D pinning of medium-sized flux bundles.

A problem in both the analysis after Maley *et al.*[43] and in terms of the GIS (Ref. 55) is the correct choice of the parameters C and C_g, respectively. C was estimated to be 20 ± 2 for the present sample. A comparison of this value with those reported in literature shows that a value of 20 is relatively high. Kung *et al.*[58] found a value of about 16 for a melt-powder-melt-growth (MPMG) YBCO sample of comparable size but little lower J_c values. $C=18$ was used to analyze another melt-texture-growth (MTG) YBCO compound.[59] Lower values are found for single crystals.[60] Also for C_g which has to be larger than C according to Eq. (10), values are usually reported below 20 (Refs. 56 and 61) in the case of thin films. But if the oxygen content in such films is reduced, an increase of C_g up to 24 can be observed.[61] If defects like oxygen vacancies[62] or irradiation damages[63] are introduced into the sample a strong increase of C was found. Furthermore van der Beek *et al.*[64] have shown that C can be written within the flux-flow model of Bardeen and Stephen as $C \sim \ln(2\rho_n BJ/B_{c2}\mu_0 d)$, where ρ_n is the normal-state resistivity. According to this equation a higher value for C is expected for a sample with higher critical current density. Taking into account that our sample has a higher disorder because of the complex pinning structure, relatively high critical current density, and reduced oxygen content, the obtained C value is at an upper limit but not unbelievably high. Fortunately a variation of both C and C_g does not seriously influence the result concerning the determination of flux creep regimes as discussed in Figs. 8 and 13.

A further problem is choosing the correct temperature dependence of the pinning potential which is taken into account by the function $g(T)$. Although there are some suggestions how this function should look, it is, however, not universal.[65] Tinkham[44] has shown that in a Ginzburg-Landau treatment from the temperature dependence of the condensation energy, the coherence length and the flux-line-lattice spacing near T_c a $(1-t)^{3/2}$, and at lower temperatures, a much flatter $(1-t^2)$ dependence is expected. Ossandon *et al.*[62] have proposed a $(1-t^2)^{3/2}$ dependence, which is a combination of both relations. Whereas $(1-t^2)$ should be the first choice, it often only leads to good results if in $t=T/T_K$ for T_K the irreversibility temperature T_{irr} is used instead of the theoretical expected transition temperature T_c.[45,58] A very thorough investigation of the $g(T)$ function was carried out by Kung *et al.*,[58] where they determined the correction factor for each temperature from the condition that adjacent temperatures should fit together as smoothly as possible. These factors were then fitted by a function $[1-(T/T_K)^2]^m$, where values for m between 0.8 and 4.5 were obtained. Especially for those samples which show a fishtail effect, extreme values for m were obtained, which cannot be explained theoretically. Such analysis always has the disadvantage that pos-
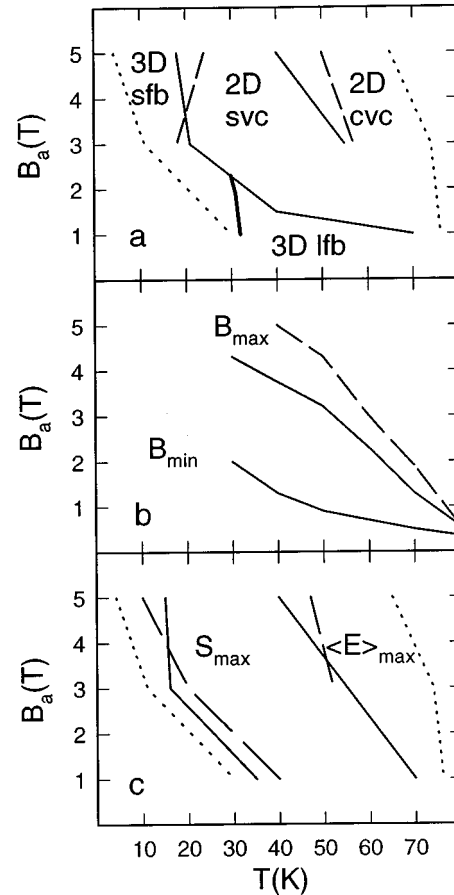

FIG. 14. (a) Phase diagram obtained from the analysis of the $U(J)$ curves (Fig. 7) in terms of collective pinning theory. At fields and temperatures outside of the fishtail regime a change from 3D pinning of small flux bundles (3D *sfb*) to pinning of large flux bundles (3D *lfb*) with increasing field and temperature is obtained. At fields and temperatures where the fishtail appears a change from 2D pinning of single vortices (2D *svc*) to collective pinning of pancakes (2D *cvc*) with increasing temperature is observed. (b) Fishtail regime characterized by the field where the fishtail starts to appear (B_{min}) and where it shows its maximum (B_{max}). (c) Field dependence of the maximum in the normalized creep rate S_{max} and of the mean effective activation energy $\langle E \rangle_{max}$ determined after Anderson (Refs. 38, 39). The area outside of the dotted lines indicates those fields and temperatures where no relaxation measurements were performed. Results of the analysis of the measurements performed before (after) the reoxygenation process are shown as dashed (solid) lines.

sible changes in the $U(J)$ characteristics, which may be caused by a change in the pinning regime, could be overlooked when they are taken only as changes of $g(T)$. Therefore we have decided not to determine $g(T)$ point by point but to choose a given function. In our case, because the low-to-medium temperature range is essential for the analysis, the function $(1-t^2)$ was chosen with $t=T/T_c$. Within our measuring accuracy no improvement is found if T_c is replaced by T_{irr} (Fig. 8).

In Fig. 14(a) the phase diagram is given, which was obtained from the analysis of the thus determined $U(J)$ relations (Figs. 7 and 9). It is characterized by a line, below which the system behaves in a three-dimensional way and above which it behaves in a two-dimensional way. Below

this line a change from pinning of small flux bundles to pinning of large flux bundles with increasing temperature is obtained. This behavior is in agreement with theoretical propositions[52] and with the experimental results obtained from the analysis of fully oxygenated melt-textured samples which show no fishtail effect.[57] At higher fields and temperatures a change from two-dimensional pinning of single pancakes to collective pinning of two-dimensional vortices is obtained. This is the regime where the fishtail is present. A comparison of this phase diagram with the one obtained from the analysis of the field dependence of the critical current density [Figs. 2 and 14(b)] indicates that the line which separates the 2D from the 3D regime is identical to $B_{\min}(T)$, which defines the onset of the fishtail. The field $B_{\max}$, which describes the maximum of the fishtail, is in the region where the change from svc to cvc in two dimensions is found. After reoxygenation the line $B_{\max}(T)$ shifts in the same direction as the border between 2D svc and 2D cvc. The changes in pinning behavior are also visible in the results of the relatively simple analysis in terms of single barrier height model [Fig. 14(c)].

In the following, the possible reasons for the obtained change in dimensionality of the pinning is discussed. Such a change from 3D to 2D pinning behavior should appear if the elastic shear energy within the planes becomes equal to the tilt energy between the planes. In that case theory[66] predicts $H_{\mathrm{cr}} \sim \phi_0 \gamma^{-2} s^{-2}$ for the crossover field, where γ is the anisotropy constant and s the distance of the CuO_2 planes. A decrease of H_{cr} with increasing anisotropy is expected from this equation. For example, such a crossover was found in the high anisotropic material Tl2201,[26] in Bi2212 single crystals,[24] in some exotic organic superconductors,[25] and in oxygen-reduced YBCO samples.[27,28,57,67,68] According to the above equation a crossover field of a few Tesla would require an anisotropy ratio between 10 and 20. For YBCO with only small oxygen reduction this is of course high, but not impossible.

Another aspect is that in such a model, where $B_{\min}$ is assumed to be correlated with a 3D to 2D transition in the pinning of the same type of pinning centers, the decrease of J_c above $B_{\max}$ is caused simply by the usual weakening of pinning, due to the suppression of the global order parameter by approaching the irreversibility line.[6] This suggests that the temperature dependence of $B_{\max}$ should be equal to the temperature dependence of the irreversibility field. Indeed, sometimes for the temperature dependence of $B_{\max}$, which can be written as $B_{\max} \sim B_0 (1-t)^n$ with $t = T/T_c$, an exponent of $n = 3/2$ is found, which resembles the temperature dependence of the irreversibility line. In contrast, in our sample the exponent changes with the temperature. For temperatures below 40 K (47 K) a value for n of 1/2 (1/2) and for higher temperatures of 1 (3/2) is obtained before (after) reoxygenation. A correlation of $B_{\max}$ with the irreversibility line does not appear to be the case. It is more reliable that $B_{\max}$ is not accidentally in the same field and temperature range where the change from 2D svc to 2D cvc appears (Fig. 14), but is casually coupled to this change in pinning behavior.

Furthermore, if a change in the relation of inter- to intra-plane coupling of vortices would be the explanation of the found 3D to 2D crossover in our sample, the change in pin-

ning should also be visible in the field dependence of the $U(J)$ relations. Whereas pinning of large bundles in 3D should lead to a H^{-3} dependence,[16,69] pinning by planar defects like twins[70] or 123-211 interfaces[71] would lead to $H^{-0.5}$. Such field scaling for all temperatures could not be found in our sample. Only between 3 and 5 T at temperatures higher than 50 K is a $H^{-0.5}$ scaling obtained. This is the region above $B_{\max}$ and $\langle E \rangle_{\max}$ where 2D cvc is dominant (Fig. 14). A similar failure of field scaling of the $U(J)$ curves in MPMG-YBCO samples with fishtail was reported by Kung et al.[58]

Out of the many possible explanations about the reason for the fishtail discussed in the introduction, most can now be ruled out. If the fishtail is caused by a matching effect, the maximum in J_c should be at that field where the flux-line-lattice spacing equals the mean defect distance d, which can be estimated from the matching field $B_m \sim \phi_0/d^2$. B_m, which should be identical with the maximum field $B_{\max}$, lies between 2 and 5 T. This leads to a mean defect spacing of about 30 to 60 nm, a dimension much lower than most of the characteristic defect lengths identified in the microstructural analysis. Only the spacing of twins around the 211 particles where their density is much higher than in the undisturbed 123 matrix, becomes lower than 1 μm. From the microstructural analysis it was further concluded that around the 211 inclusions large stresses are present.[31] These stresses are highly inhomogeneous and maximal at the 123-211 interfaces. Tensile stresses in the c direction up to 290 MPa and between 50 and 100 MPa in the ab plane are obtained. There are further shear stresses in the c direction of about 160 MPa. It has been argued that the large strain fields together with the positional disordered regions around the 211 particles in melt-textured YBCO samples lead to a high dislocation density. A density of 10^{10} cm^{-2} as found in similar melt-textured samples[72] corresponds to a mean distance of about 100 nm, which would also be in the correct order of magnitude. But in the case of matching, the fishtail is expected to be both independent of temperature and oxygen content, which is contrary to the findings in our sample.

The role of oxygen defects in the appearance of the fishtail was investigated by the reoxygenation process. In the collective pinning theory the critical current density is proportional to some power of the density of the pinning centers. If the pinning centers are oxygen vacancies J_c should be reduced after the reoxygenation process. The reduction in J_c which correspond to a reduction in the width of the hysteresis loops is clearly visible in the fishtail regime (Fig. 1). But below $B_{\min}(T)$ the width and therefore J_c are not changed by the reduction in the number of oxygen defects.

This points to the existence of two different types of pinning centers, one responsible for the fishtail and related to the oxygen content, and one insensitive to the reoxygenation process and dominating the field and temperature region outside of the fishtail regime. The absence of field scaling of $U(J)$ for all temperatures may also be an indication of the existence of different pinning mechanisms caused by different types of pinning centers in the sample.

The existence of two types of pinning centers is also found in the analysis of the relaxation measurements in terms of activation energy distributions (inset, Fig. 6). Whereas at 1 T only one peak is found in the distribution function, a

second peak at higher temperatures appears for 3 and 5 T. Although the value of the energy where the second peak appears cannot be taken as a representative one for the true pinning potential well height because of the crude assumptions (e.g., the linear Anderson-Kim ansatz for the energy current relation) which are underlaid to such type of analysis, a comparison of the relative strengths and statements concerning relative changes of activation energies with temperature and field are usually correct.[73–79]

Further evidence of two different pinning centers follows from the analysis of the dynamic relaxation rates in terms of the GIS. If the fishtail is only a dynamic effect and not caused by a dimensional crossover or by the existence of other pinning centers, it should be visible only in J_c and not in the true critical current density J_{ct}.[80] Interestingly the hump which appears in the temperature dependence of the apparent critical current density J_c (Fig. 3) at higher fields is also visible in the temperature dependence of the true critical current density J_{ct} (Fig. 12).

The background pinning—dominant in the field and temperature range before the fishtail sets in—is also expected to change with oxygen content (a strong increase in the number of oxygen defects also induces a 2D pinning character[57,67,68]). The alteration in oxygen content during the reoxygenation process is, however, too low to make this change visible. This background pinning behaves as usual in YBCO in a 3D way, but in contrast to findings in YBCO samples without a fishtail, where often single vortex creep is found, a change from small- to large-flux-bundle pinning takes place when field and/or temperature are increased. The crossover field from single vortex pinning to small-flux-bundle pinning B_{sb} is determined by the condition $L_c = a_0 \gamma^{-1}$, where $a_0 = (\phi_0/B_{sb})^{1/2}$ is the average distance between the vortices. L_c is the c axis correlation length and γ is the anisotropy parameter. In pure YBCO films the crossover field was estimated to be ~ 2 T.[61] In our sample the anisotropy parameter γ is much higher due to a much higher disorder. Therefore for a given correlation length L_c a lower transition field B_{sb} is to be expected. Because our lowest field for the relaxation measurements was 1 T, it is not surprising that a single vortex regime could not be detected.

In contrast to the background pinning the pinning centers responsible for the fishtail are influenced more strongly by a change in oxygen content. It should be mentioned that not only the change in content, but also the arrangement of the oxygen defects may be important for the appearance of the fishtail.[8,9] Reduction in the number of oxygen defects re-

duces the fishtail. These pinning centers behave in a 2D way. This can be concluded from the analysis of the $U(J)$ curves in terms of collective pinning theory, from the $H^{-0.5}$ dependence of the $U(J)$ curves at high temperatures, and also from the determination of the temperature dependence of the true critical current density. In the activation energy distribution the peak which corresponds to these pinning centers appears at higher energies than the background-pinning peak.

The consequence of the higher energy together with the flatter field dependence of $U(J)$, in comparison to the one for the background pinning, is the appearance of the fishtail. These pinning centers seem to be some kind of planar defect. This is in agreement with the fact that a field scaling of $H^{-0.5}$ is predicted both in the case of twin boundary pinning[70] as well as pinning at the 123-211 interface,[71] which are both planar defects. Finally, it should be mentioned that Sandiumenge *et al.*[81] published a very detailed investigation of the microstructure in melt-textured samples with a fishtail effect, where they found indications for such planar oxygen defects.

VII. CONCLUSIONS

Magnetic hysteresis and flux creep investigations on a melt-textured YBCO sample showing a fishtail effect were performed before and after changing the oxygen content. The measurements were analyzed in terms of the classical flux creep theory from Anderson, in terms of activation energy distributions as well as by analyzing the hysteresis loops recorded with different field sweep rates within the generalized inversion scheme. Within the collective pinning theory the existence of two different types of pinning centers can be found. One is dominant in the low-field regime and is associated with usual 3D behavior. A change from small- to large-flux-bundle pinning is obtained when temperature and field are increased; no influence of a small change in oxygen content could be observed. The other pinning centers dominate at higher fields and temperatures where the fishtail appears. These are planar defects with higher activation energies. They are strongly influenced by changing oxygen content and show a 2D pinning behavior.

ACKNOWLEDGMENTS

[1] A. M. Campbell and J. E. Evetts, Adv. Phys. **21**, 199 (1972).

[2] M. Däumling, J. M. Seuntjens, and D. C. Larbalestier, Nature (London) **346**, 332 (1990).

[3] M. S. Osofsky, J. L. Cohn, E. F. Skelton, M. M. Miller, R. J. Soulen, Jr., S. A. Wolf, and T. A. Vanderah, Phys. Rev. B **45**, 4916 (1992).

[4] C. Keller, H. Küpfer, A. Gurevich, R. Meier-Hirmer, T. Wolf, R. Flükiger, V. Selvamanickam, and K. Salama, J. Appl. Phys. **68**, 3498 (1990).

[5] J. L. Vargas and D. C. Larbalestier, Appl. Phys. Lett. **60**, 1741 (1992).

[6] J. G. Ossandon, J. R. Thompson, D. K. Christen, B. C. Sales, H. R. Kerchner, J. O. Thomson, Y. R. Sun, K. W. Lay, and J. E. Tkaczyk, Phys. Rev. B **45**, 12 534 (1992).

[7] A. Erb, J.-Y. Genoud, F. Marti, M. Däumling, E. Walker, and R. Flükiger, J. Low Temp. Phys. **105**, 1023 (1996).

[8] H. Theuss and H. Kronmüller, Physica C **177**, 253 (1991).

[9] B. Revaz, A. Junod, A. Mirmelstein, A. Erb, J.-Y. Genoud, and

G. Triscone, Czech. J. Phys. **46**, 1205 (1996).

[10] Ming Xu, D. K. Finnemore, G. W. Crabtree, V. M. Vinokur, B. Dabrowski, D. G. Hinks, and K. Zhang, Phys. Rev. B **48**, 10 630 (1993).

[11] A. Wisniewski, R. Szymczak, R. Puzniak, M. Baran, J. Karpinski, and H. Schwer, Czech. J. Phys. **46**, 1651 (1996).

[12] G. Yang, P. Shang, S. D. Sutton, I. P. Jones, J. S. Abell, and C. E. Gough, Phys. Rev. B **48**, 4054 (1993).

[13] E. H. Brandt, Rep. Prog. Phys. **58**, 1465 (1995).

[14] E. H. Brandt, Int. J. Mod. Phys. B **5**, 751 (1991).

[15] C. D. Wei, Z. X. Liu, H. T. Ren, and L. Xiao, Physica C **260**, 130 (1996).

[16] L. Kruisin-Elbaum, L. Civale, V. M. Vinokur, and F. Holtzberg, Phys. Rev. Lett. **69**, 2280 (1992).

[17] L. F. Cohen, J. R. Laverty, G. K. Perkins, A. D. Caplin, and W. Assmus, Cryogenics **33**, 352 (1993).

[18] N. Chikumoto, M. Konczykowski, N. Motohira, and A. P. Malozemoff, Phys. Rev. Lett. **69**, 1260 (1992).

[19] A. A. Zhukov, H. Küpfer, S. N. Gordeev, W. Jahn, T. Wolf, V. I. Voronkova, A. Erb, G. Müller-Vogt, H. Wühl, H. J. Bornemann, K. Salama, and D. F. Lee, in *Proceedings of the 7th International Workshop on Critical Currents in Superconductors*, edited by H. W. Weber (World Scientific, Singapore, 1994), p. 229.

[20] M. R. Koblischka, A. J. J. van Dalen, Th. Schuster, M. Leghissa, and M. Jirsa, Physica C **235−240**, 2839 (1994).

[21] O. B. Hyun, M. Yoshida, T. Kitamura, and I. Hirabayashi, Physica C **258**, 365 (1996).

[22] A. I. Larkin and Yu. N. Ovchinnikov, J. Low Temp. Phys. **34**, 409 (1979).

[23] R. Hergt, R. Hiergeist, and A. Erb, J. Alloys Compd. **195**, 431 (1993).

[24] C. D. Dewhurst, R. A. Doyle, D. A. Cardwell, A. M. Campbell, and G. Balakrishnan, in *Proceedings of the 2nd European Conference on Applied Superconductivity (EUCAS 95)*, edited by D. Dew-Hughes IOP Conf. Proc. No. **148** (Institute of Physics and Physical Society, London, 1995), p. 291.

[25] F. Zuo, S. Khizroev, G. C. Alexandrakis, J. A. Schlueter, U. Geiser, and J. M. Williams, Phys. Rev. B **52**, R13 126 (1995).

[26] F. Zuo, S. Khizroev, G. C. Alexandrakis, and V. N. Kopylov, Phys. Rev. B **52**, R755 (1995).

[27] J. Deak, L. Hou, P. Metcalf, and M. McElfresh, Phys. Rev. B **51**, 705 (1995).

[28] X. G. Qiu, B. Wuyts, M. Maenhoudt, V. V. Moshchalkov, and Y. Bruynseraede, Phys. Rev. B **52**, 559 (1995).

[29] R. Meier-Hirmer, H. Küpfer, and H. Scheurer, Phys. Rev. B **31**, 183 (1985).

[30] N. Pellerin, M. Gervais, and P. Odier, in *Layered Superconductors: Fabrication, Properties, and Applications,* edited by D. T. Shaw *et al.*, MRS Symposia Proceedings No. 275 (Materials Research Society, Pittsburgh, 1992), p. 537.

[31] P. Diko, N. Pellerin, and P. Odier, Physica C **247**, 169 (1995).

[32] L. Pust, J. Kadlecová, M. Jirsa, and S. Durcok, in *Proceedings of the International Conference on the Nature and Properties of High-Temperature Superconductors, Wroclaw, Poland, 8-10 June, 1989* (Institute for Low-Temperature and Structure Research, Polish Academy of Sciences, Wroclaw, 1989), Abstract C-7.

[33] L. Pust, J. Kadlecová, M. Jirsa, and S. Durcok, Low Temp. Phys. **78**, 179 (1990).

[34] H. G. Schnack, R. Griessen, J. G. Lensink, C. J. van der Beek, and P. H. Kes, Physica C **197**, 337 (1992).

[35] S. Senoussi, J. Phys. (France) III **2**, 1041 (1992).

[36] M. Reissner, W. Steiner, R. Stroh, S. Hörhager, W. Schmid, and W. Wruss, Physica C **167**, 495 (1990).

[37] D. X. Chen and R. B. Goldfarb, J. Appl. Phys. **66**, 2489 (1989).

[38] P. W. Anderson, Phys. Rev. Lett. **9**, 309 (1962).

[39] P. W. Anderson and Y. B. Kim, Rev. Mod. Phys. **36**, 39 (1964).

[40] M. Reissner, R. Ambrosch, and W. Steiner, in *Relaxation in Complex Systems and Related Topics*, edited by I. A. Campbell and C. Giovanella (Plenum, New York, 1990), p. 99.

[41] C. W. Hagen, R. Griessen, and E. Salomons, Physica C **157**, 199 (1989).

[42] M. R. Beasley, R. Labusch, and W. W. Webb, Phys. Rev. **181**, 682 (1969).

[43] M. P. Maley, J. O. Willis, H. Lessure, and M. E. McHenry, Phys. Rev. B **42**, 2639 (1990).

[44] M. Tinkham, Phys. Rev. Lett. **61**, 1658 (1988).

[45] M. E. McHenry, S. Simizu, H. Lessure, M. P. Maley, J. Y. Coulter, I. Tanaka, and H. Kojima, Phys. Rev. B **44**, 7614 (1991).

[46] E. Zeldov, N. M. Amer, G. Koren, A. Gupta, M. W. McElfresh, and R. J. Gambino, Appl. Phys. Lett. **56**, 680 (1990).

[47] M. V. Feigel'man, V. B. Geshkenbein, A. I. Larkin, and V. M. Vinokur, Phys. Rev. Lett. **63**, 2303 (1989).

[48] M. V. Feigel'man, V. B. Geshkenbein, and A. I. Larkin, Physica C **167**, 177 (1990).

[49] V. M. Vinokur, P. H. Kes, and A. E. Koshelev, Physica C **168**, 29 (1990).

[50] V. M. Vinokur, P. H. Kes, and A. E. Koshelev, Physica C **248**, 179 (1995).

[51] M. V. Feigel'man, V. B. Geshkenbein, and V. M. Vinokur, Phys. Rev. B **43**, 6263 (1991).

[52] G. Blatter, M. V. Feigel'man, V. B. Geshkenbein, A. I. Larkin, and V. M. Vinokur, Rev. Mod. Phys. **66**, 1125 (1995).

[53] H.-H. Wen, R. Griessen, D. G. de Groot, B. Dam, and J. Rector, J. Alloys Compd. **195**, 427 (1993).

[54] M. Jirsa, L. Pust, H. G. Schnack, and R. Griessen, Physica C **207**, 85 (1993).

[55] H. G. Schnack, R. Griessen, J. G. Lensink, and H.-H. Wen, Phys. Rev. B **48**, 13 178 (1993).

[56] H.-H. Wen, H. G. Schnack, R. Griessen, B. Dam, and J. Rector, Physica C **241**, 353 (1995).

[57] M. Reissner, W. Steiner, C. Czurda, H. W. Weber, A. Wisniewski, P. X. Zhang, and L. Zhou, *Proceedings of the 7th International Workshop on Critical Currents in Superconductors*, edited by H. W. Weber (World Scientific, Singapore, 1994), p. 451.

[58] P. J. Kung, M. P. Maley, M. E. McHenry, J. O. Willis, M. Murakami, and S. Tanaka, Phys. Rev. B **48**, 13 922 (1993).

[59] S. Y. Ding, Z. Y. Zeng, J. Li, and X. X. Yao, Physica C **235−240**, 2895 (1994).

[60] D. Shi and S. Salem-Sugui, Jr., Phys. Rev. B **44**, 7647 (1991).

[61] A. J. J. van Dalen, R. Griessen, S. Libbrecht, Y. Bruynseraede, and E. Osquiguil, Phys. Rev. B **54**, 1366 (1996).

[62] J. G. Ossandon, J. R. Thompson, D. K. Christen, B. C. Sales, Y. Sun, and K. W. Lay, Phys. Rev. B **46**, 3050 (1992).

[63] H. S. Lessure, S. Simizu, B. A. Baumert, S. G. Sankar, M. E. McHenry, M. P. Maley, J. R. Cost, J. O. Willis, IEEE Trans. Magn. **27**, 1043 (1991).

[64] C. J. van der Beek, G. J. Nieuwenhuys, P. H. Kes, H. G. Schnack, and R. Griessen, Physica C **197**, 320 (1992).

[65] M. Suenaga, A. Ghosh, T. Asano, R. L. Sabatini, and A. R. Moodenhbaugh, in *High Temperature Superconductors* (Materials Research Society, Pittsburgh, 1987), Vol. EA-11, p. 247.

[66] L. I. Glazman and A. E. Koshelev, Phys. Rev. B **43**, 2835 (1991).

[67] C. Czurda, H. W. Weber, A. Wisniewski, P. X. Zhang, and L. Zhou, in *Applied Superconductivity*, edited by H. C. Freyhardt (DGM Informationsgesellschaft, 1993), p. 795.

[68] A. Wisniewski, C. Czurda, H. W. Weber, M. Baran, M. Reissner, W. Steiner, P. X. Zhang, and L. Zhou, Physica C **266**, 309 (1996).

[69] B. Martínez, X. Obradors, A. Gou, V. Gomes, S. Piñol, J. Font-cuberta, and H. Van Tol, Phys. Rev. B **53**, 2797 (1996).

[70] D. R. Nelson and V. M. Vinokur, Phys. Rev. B **48**, 13 060 (1993).

[71] M. Murakami, S. Gotoh, H. Fujimoto, K. Yamaguchi, N. Koshizuka, and S. Tanaka, Supercond. Sci. Technol. **4**, S43 (1991).

[72] M. Ullrich, D. Müller, K. Heinemann, L. Niel, and H. C. Freyhardt, Appl. Phys. Lett. **63**, 406 (1993).

[73] C. C. Almasan, C. L. Seaman, Y. Dalichaouch, and M. B. Maple, Physica C **174**, 93 (1991).

[74] M. Mittag, R. Job, and M. Rosenberg, Physica C **174**, 101 (1991).

[75] M. Reissner and W. Steiner, Supercond. Sci. Technol. **5**, S367 (1992).

[76] M. Reissner, W. Steiner, W. Kritscha, F. M. Sauerzopf, and H. W. Weber, in *Progress in High Temperature Superconductivity*, edited by M. Baran, W. Gorzkowski, and H. Szymczak (World Scientific, Singapore, 1992), Vol. 30, p. 239.

[77] H. Theuss, Physica C **208**, 155 (1993).

[78] V. Hardy, A. Ruyter, J. Provost, D. Groult, and Ch. Simon, Physica C **224**, 143 (1994).

[79] M. Reissner, G. Hadaier, W. Steiner, G. Fuchs, A. Gladun, and K. Fischer, IEEE Trans. Magn. **30**, 1175 (1994).

[80] A. J. J. van Dalen, M. R. Koblischka, R. Griessen, M. Jirsa, and G. Ravi Kumar, Physica C **250**, 265 (1995).

[81] F. Sandiumenge, N. Vilalta, S. Piñol, B. Martínez, and X. Obradors, Phys. Rev. B **51**, 6645 (1995).